SECTION 4

ENERGY

ASME District F - Early Career Technical Conference Proceedings
ASME District F - Early Career Technical Conference, ASME District F – ECTC 2013
November 2 – 3, 2013 - Birmingham, Alabama USA

ENERGY USAGE MODELING AND MEASUREMENTS FOR AN ELECTRIC MOTORCYCLE ON A CROSS COUNTRY ROUTE

Will K. Hays, Robert J. Prins
James Madison University
Harrisonburg, VA, USA

ABSTRACT

Popular perceptions of electric vehicles include presumed limitations associated with range, recharging times, and availability of charging sites. In order to demonstrate the current state of capability of a modern electric motorcycle for long distance travel, Team Moto-Electra conducted a cross-country trip spanning the continental United States in three and a half days. Engineering students from James Madison University helped to prepare the bike and also provided support during the crossing. The intention of the effort was to demonstrate the range and recharge capability of a modern electric motorcycle and to validate a road load-based energy usage model that a student developed for the motorcycle. In order to decouple the limitations of range and recharging times from charging site availability, a generator provided recharging power during the stops along the 2366 mile route.

This paper includes technical details of the motorcycle and the road load energy model as well as validation of the model. During the trip the team logged battery pack voltage and output current along with GPS tracking data. Processed GPS tracking data provides speed and elevation information which, when combined with the energy usage model, predicts the energy required from the battery pack. The model was then validated by comparisons of the predicted energy usage to the measured energy usage determined from the battery pack voltage and current data. The cross country nature of the trip provided a significant amount of data for model validation as well as general characterization of the trip in terms of speed, power consumption, and road slope.

INTRODUCTION

Increased interest in the high performance aspects of electric motorcycles has helped to build the market for two wheeled electric vehicles. Electric motorcycles now compete in drag racing, road racing, hill climb, and motocross. Participation in endurance racing has not been as significant due to limitations related to battery charging. However, application to real life motorcycle markets beyond commuting requires consideration of charging as a fundamental component of a trip. A cross-country trip by electric motorcycle (Moto Electra endurance racer) was undertaken in order to address perceptions of electric motorcycle range, experience potential limitations first hand, and to gather data related to such a trip. The 84.5 hour cross-country trip occurred on June 3-6 2013 and extended from the Atlantic Ocean (beachfront in Jacksonville, FL) to the Pacific Ocean (Santa Monica, CA) for a total of 2,365.8 miles; primarily following Interstate 10. In order to distinguish issues related to motorcycle range from issues associated with charging stations, the team carried its own generator and charging equipment. Charging occurred prior to the start of the trip and at 25 stops during the trip; data collected along the way was divided into 26 segments, averaging about 91 miles per segment, with charging points defining the end of a given segment and the beginning of the following segment. The focus of this paper is the presentation and analysis of the data gathered along the trip.

The motorcycle was equipped with a data acquisition system that recorded power draw from the battery pack as well as GPS data (including speed and elevation). Data from the GPS was used as input to a road load-based energy usage model to provide an estimate of energy usage for each trip segment. Battery pack voltage and current draw were also monitored to provide a direct measurement of energy usage for each trip segment. The model-based estimate was compared to the direct measurement to test model validity. GPS and battery pack data were also used to provide summary details of the trip that could be used to inform drivetrain and battery pack design. This data is presented in the form of histograms of vehicle speed, power draw, and road gradient.

The use of a GPS to provide measurements of vehicle speed and elevation changes, in order to determine vehicle load conditions, is a key component in vehicle testing. Some examples include a GPS-based method for experimental determination of vehicle mass, drag coefficient, and rolling resistance [1]; use of a GPS for modeling losses due to aerodynamic drag, drivetrain friction, and tires [2]; and use of a GPS in conjunction with portable emissions monitoring equipment to monitor emissions characteristics in on-road driving conditions [3]. All three examples use GPS data to provide input into a commonly accepted model of road load force that estimates the road load force at specific points along a travel path. Since GPS information used for such purposes is typically updated every second, a dense set of road load

force estimates is obtained for a given trip. In previous work, Prins [4] applied a GPS-based method for the validation of a road load model of an electric utility vehicle using a similar approach to that described in this work.

Technical Details of Motorcycle

The Moto-Electra endurance racer is a custom built electric motorcycle constructed by Brian Richardson, team manager of Moto-Electra LLC. The bike is made of a combination of off-the-shelf drive components, purpose-built battery packs, and a custom fabricated chassis. The drivetrain is an AC 35 kit from Hi Performance Electric Vehicle Systems consisting of a Curtis 1238-7601 controller and an AC-35 High Performance Electric Vehicle Systems three phase induction motor. The motor is connected to the rear wheel via a 16/50 sprocket combination providing a final drive ratio of 0.32. The wheels are 18" BlackStone Tek (BST) carbon fiber fitted with ceramic bearings. The rear tire is a Dunlop Street Smart 160/60ZR17, with measured circumference of 78" circumference; at the typical travel speed of 60 MPH the motor turned 2,540 RPM.

The endurance racer was fitted with two battery packs, a primary pack which fit within the frame of the chassis and an auxiliary pack which was mounted to the rear of the rider in a saddlebag configuration. The primary pack consists of 32 100Ah Kokam SLPB High Power cells while the auxiliary pack consists of 32 100 Ah Kokam SLPB High Energy cells. The auxiliary pack was purchased in used condition; subsequent bench testing revealed that it had about 90% of the energy storage capacity of the primary pack. Although the charge/discharge damage threshold for the cells is 4.2V/2.8V, for bench testing the applied charge/discharge limits were 4.1V/3.4V per cell.

During cross country operation typical usage limits were a more conservative 4.0/3.6V per cell; this was done to minimize the potential for the pack to become unbalanced. Balancing of the cells in each pack was achieved with a battery management system during the charge cycle, with balancing typically keeping the charged cells within 20mV of each other. The packs were not connected to each other; during vehicle operation either one of the packs could be connected as the energy source while the other pack was disconnected, thus permitting full spare capacity. Switching between packs was a manual operation that required a brief stop.

The chassis was constructed by FrameCrafters Performance Motorcycle Fabricators in Union, IL and is modeled on a 1966 Norton Atlas "featherbed" chassis with allowances made to accommodate modern racing tires and an electric motor.

METHODOLOGY

To reasonably predict the energy usage of an electric motorcycle, a model is required of the vehicle and the route which the vehicle will travel. This model was used to analyze the data which was then compared to the measured energy usage. The measurement of the energy used was obtained by monitoring the battery pack output energy during the study. This section describes the vehicle model, the hardware used to collect the data and how the data was collected and analyzed.

Model

The model in this study consists of all the forces aligned with the direction of travel acting on the vehicle based on Newton's second law as described by Gillespie [5]. Rearrangement of the force equation to isolate the force needed to be supplied by the vehicle to the road is shown in equation 1:

$$F_{RL} = \eta * (F_{RR} + F_D + F_G + F_a) \quad (1)$$

where,

F_{RL}= total road load force needed by vehicle
η= lumped efficiency of controller, motor, and drive train
F_{RR}= force due to rolling resistance
F_D= force due to aerodynamic drag
F_G= force due to gravity (due to road gradient)
F_a = force due to acceleration in the direction of travel

Rolling resistance addresses the resistive forces due to the contact between the tire and the road; aerodynamic drag is the force due to wind resistance; the force due to gravity accounts for the change in elevation due to road gradient; and the force of acceleration accounts for the change in speed in the direction of travel. Equation 1 can be expanded to show the terms associated with each force as shown in Equation 2:

$$F_{RL} = \eta(f_r * W + \frac{1}{2} * \rho * v^2 * C_D * A + W * \sin(\emptyset) + m * a) \quad (2)$$

where,

f_r- Rolling Resistance Coefficient
W-Weight of vehicle and rider
ρ-Density of Air
v-Velocity of vehicle
C_D-Aerodynamic Drag Coefficient
A-Cross-sectional Area of vehicle and rider
$\emptyset$-Angle of the road surface
m-Mass of vehicle and rider
a- Acceleration of vehicle

Due to constraints not allowing for wind speed measurements to be taken from the motorcycle for the application of this model wind speed was neglected and a constant value of air density was applied for the entire trip.

To determine the rolling resistance coefficient, a formula was used as shown in equation 3[6]:

$$f_r = 0.0085 + \frac{0.018}{p} + \frac{1.59*10^{-6}}{p} * v^2 \quad (3)$$

where,

p- tire pressure in bars
v-Velocity of vehicle

The terms in equations 2 and 3 include constant parameters that are directly measureable and variable parameters that could be constantly monitored during the trip, as shown in table 1. The density of air was calculated using standard pressure of 101.325 kPa and an average temperature from the trip of 29.4˚C (85˚F) [5].

Table 1. Road Load Variables, Values, and sources

Label	Variable	Value	Unit	Source
η	Efficiency of controller, motor, and drive train	0.84	N/A	Estimation based on data provided by manufacturer [8]
f_r	Rolling resistance coefficient	Varies with velocity	N/A	Calculation[6] based on GPS speed input
W	Weight of vehicle and rider	900	lb	Measurement of vehicle and rider
ρ	Density of air	1.167	Kg/m^3	Calculation [5] based on standard pressure and 85°F
v	Vehicle velocity	Varies continuously	m/s	GPS data
C_D	Aerodynamic drag coefficient	0.45	N/A	Mid-range of book value for similar vehicle[6]
A	Cross-sectional area	0.9852	m^2	Measurement of vehicle and rider
$\emptyset$	Angle of road surface	Varies continuously	Radians	Sequential GPS elevation data
m	Mass	408.23	kg	Directly calculated from weight
a	Acceleration of vehicle	Varies continuously	m/s^2	Sequential GPS speed data
p	Tire pressure	2.7579	bar	periodic tire pressure measurements

Data Acquisition

Table 1 indicates that four of the model parameters vary continuously, and their values are based on GPS data. In order to have a continuous set of values for these parameters, GPS data was gathered at a rate of 1 Hz using a GRIN Technologies Cycle Analogger with GPS receiver and stored on a SD card. Pack voltage and current measurements were also logged at a rate of 1Hz in order to continuously monitor energy usage. Pack voltage measurement was conditioned with a GRIN Technologies Cycle Analyst unit (CA-HC) and logged by the Analogger. Pack current was measured with a Honeywell CSN "loop" sensor whose output was converted to a voltage signal that was logged with the Analoggers' 0-3.3V analog input channel. The stored GPS data included the $GPRMC (Recommended minimum specific GPS/transit data) and $GPGGA (Global Positioning System fix data) NMEA sentences [7]. The NMEA sentences were interpreted as needed to provide vehicle speed and elevation.

Data Collection Protocol

To record all of the data a general protocol was set up for the cross-country trip. Whenever the motorcycle was making a stop to charge, the rider would turn the key of the motorcycle to the off position which would stop the Cycle Analogger. The data from the Cycle Analogger was then transferred from the SD card to a laptop computer, and then the Cycle Analogger was cleared to make sure there would never be a conflict of overwriting the data. After all the data had been transferred off of the Cycle Analogger, it was then set back up to turn on when the motorcycle's key was turned back to the on position.

Data Analysis

After the three and a half day trip the data was analyzed. This was done by converting the data from text documents into Excel worksheets. Raw NMEA sentences (GPS data) were filtered to extract the pertinent information. For this analysis, elevation data was extracted from $GPGGA sentences; the time stamp, validity flag, latitude/longitude, speed in knots and date stamp were extracted from $GPRMC sentences [7].

Once the data was filtered to extract only information necessary for the model, each one second interval of each trip segment was analyzed to determine road load using the model equations, constant values as shown in table 1, and variables monitored by the data acquisition system. The angle of the road surface ($\emptyset$) was calculated using speed in m/s and the elevation of sequential GPS as shown in Equation 4:

$$\emptyset = tan^{-1}\left(\frac{h_f - h_i}{v}\right) \quad (4)$$

where,

h_f=elevation at current data set

h_i= elevation at previous sequential data set

v= velocity at current data interval

Acceleration was calculated using the change in speed (m/s) from a sequential GPS data

Given the calculated road load force on each data interval, the work required over the interval was determined by multiplying by the distance traveled during the interval.

RESULTS

The results of this effort include comparisons between projected and actual energy usage as well as histograms of speed, road slope and power output for the entire trip.

In order to determine both the projected and measured energy usage for each trip segment, data for each segment was analyzed as shown in Figure 2. Figure 2a shows cumulative

energy vs. time as calculated by the model and as measured at the battery pack for trip segment 21 (San Simon, AZ to Benson, AZ). Figure 2b shows the corresponding speed and elevation data.

The projected energy usage shown in Figure 2a is based on the model in equation 2 and is therefore strongly dependent on speed and road slope. Road slope is observed in Figure 2b as the change in the elevation curve between sequential data points. During times of constant speed and constant road slope the cumulative energy graph is observed to also maintain a constant slope, as expected. As speed or slope is increased the slope of the cumulative energy curve likewise increases. Figure 2b also shows times where the cumulative energy remains constant for several seconds; these times correspond to when the vehicle was stopped for battery pack changeover.

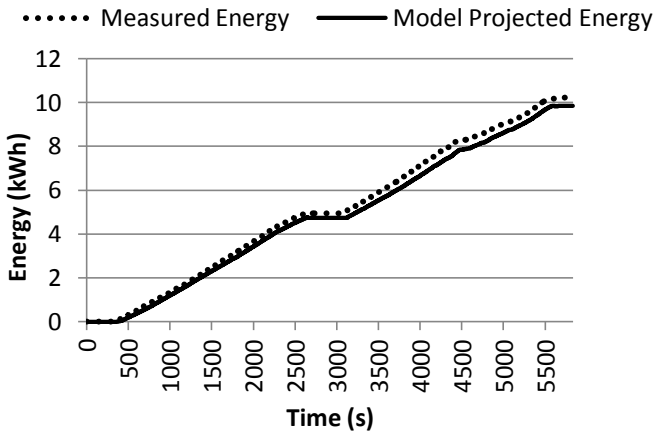

(a) Model Projected and Measured Energy Usage

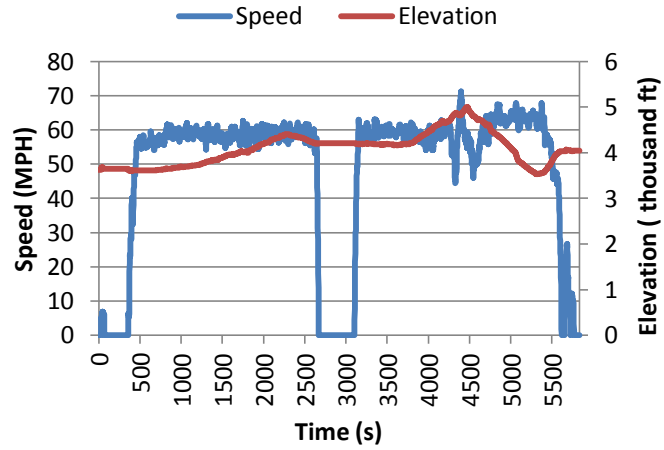

(b) Elevation and Speed Profiles

Figure 2. Model Projected and Measured Energy and Underlying Speed and Elevation for Trip Segment 21

The total measured and projected energy for trip segment 21 is determined from the final points on Figure 2a. These are 10.23 kWh cumulative measured energy usage as compared to 9.98 kWh projected energy usage. This leads to a difference of -3.8% using the measured energy total as a base. This analysis was carried out for each trip segment; the total measured and projected energy for each trip segment is shown in Figure 3a. Figure 3b shows the relative difference between the measured energy usage and the projected energy usage as a percentage.

Figure 3a demonstrates that each trip segment typically required 11 kWh, but that energy usage ranged between 5 and 17 kWh. Absolute differences between measured and projected energy usage averaged 5.2% and ranged from -11.2% to 10.9%. The amount of energy required to make the entire coast to coast trip was predicted to be 264.76 kWh and measured to be 270.64 kWh, a difference of -2.17%. On a per mile basis the motorcycle required 0.114 kWh per mile.

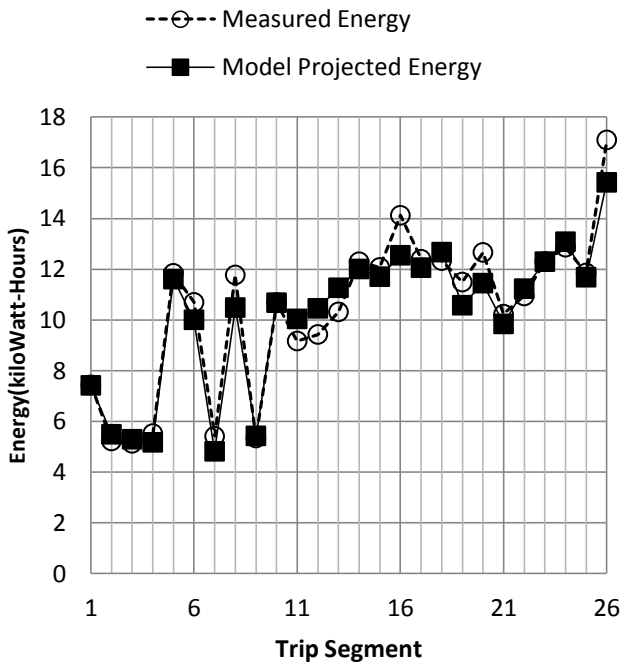

(a) Model Projected and Measured Energy Usage

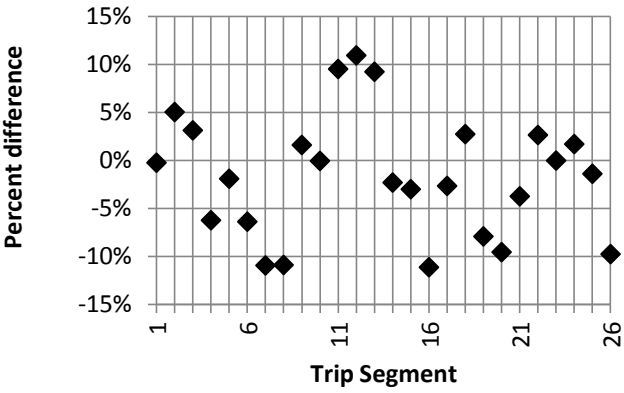

(b) Percent Difference between Model Projected and Measured Energy Usage

Figure 3. Model Project and Measured Energy Usage and Percent Difference for all Trip Segments

In addition to model verification, the data collected during the trip can provide a synopsis of environmental and operating

parameters to inform drivetrain and battery pack design. Of particular interest are road grade, travel speeds, and power draw. These data are presented as histograms that show the frequency of occurrence of a range of values in terms of percent of total trip time. For instance, Figure 4 shows the speed histogram for the entire trip. It can be seen that 23% of the trip time was spent between 57.5 and 60 MPH, and 82% of the trip time was spent between 52.5 and 65 MPH.

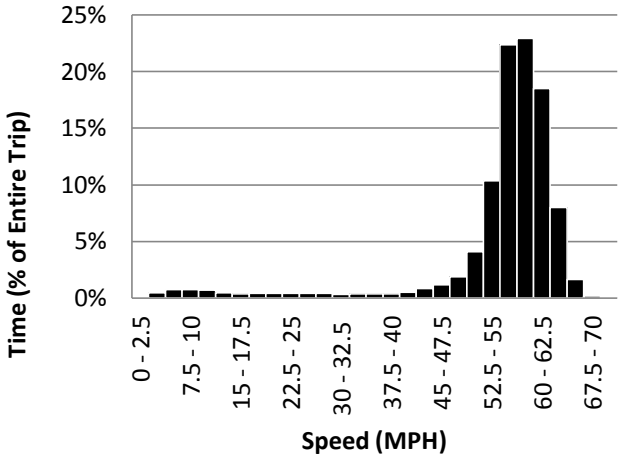

Figure 4. Speed Histogram

Figure 5 shows a histogram of the battery pack power draw as recorded by the data acquisition system (pack voltage and current). It can be seen that the most common power draw was between 7,000 and 7,500 W while 66.5% of the time the power draw was between 5,000 and 10,000 W.

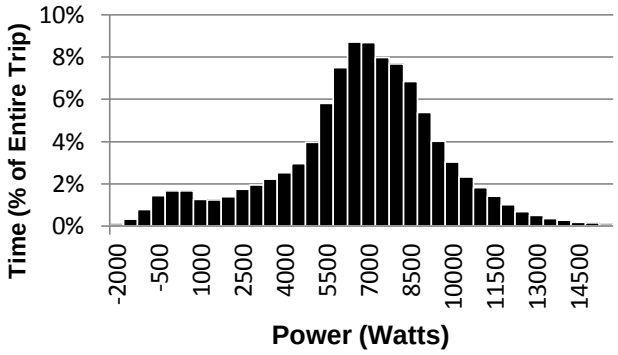

Figure 5. Power Histogram

Figure 6 shows a histogram of the road grade experienced on the trip. It can be seen that the most common grade lies between -0.5% and 0.5% (nearly level ground). More than 98% of the grades fall within ±5% as expected on an interstate.

DISCUSSION

In general the road load model accurately predicts energy usage during the trip. Energy usage for most of the trip segments is predicted to within ±5% and all of the segments are predicted to within ±11%. While this is considered a good result, it should be noted that the trip segments were generally similar and typically consisted of nearly constant cruising speeds (~60 MPH) with a few exceptions due to traffic conditions. For instance, Figure 2b shows a dip and subsequent spike of speed while the elevation is increasing continuously at ~4300 s. This was due to initially getting caught behind slower traffic while climbing a hill, and then over-speeding while executing a pass. Although this was not an isolated event, it was not typical, and it should be noted that this work does not include significant testing of the model in typical urban driving conditions.

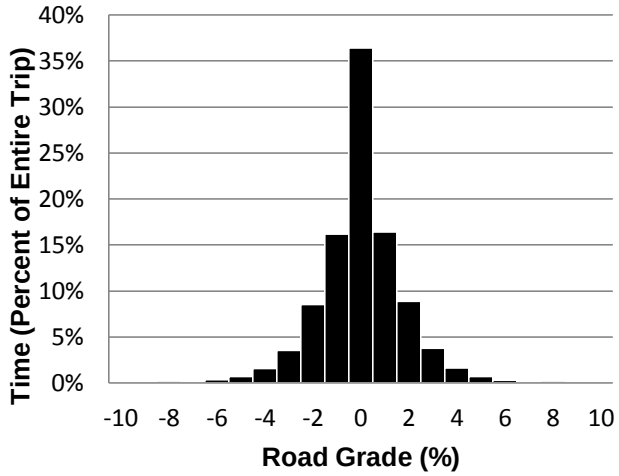

Figure 6. Road Grade Histogram

Table 1 indicates that the lumped efficiency factor, η, is estimated from manufacturer data. This is listed as an estimate since manufacturer data is not available for the exact operating conditions observed during the trip. Table 1 further indicates that the drag coefficient, C_D, is based on a book value for similar vehicles. Since most of the travel occurred at similar speed (see Figure 4) it would be possible for an error in the efficiency term to be masked by an offsetting error in the drag coefficient. Confidence in these terms could be increased by using direct measurements rather than estimates and book values. For instance, dynamometer testing could improve confidence in the efficiency term and wind tunnel or coast down testing could increase confidence in the drag coefficient. The authors intend to follow up with dynamometer testing of the vehicle and may have opportunity to perform coast down tests.

Another source of uncertainty that can be addressed in the future is related to air density. For this work, a single value of air density, ρ, was applied for the entire trip. Although it is unlikely that the air density varied enough to have significant effect on model predictions, that assumption can be verified by mining climatological data from weather stations along the route using the NOAA database. Such data could also be used to provide estimates of wind speed and direction which could then be applied to the velocity term in equation 2; this would affect the drag portion of the road load force.

Figure 3, which displays the energy usage for each trip segment, shows that the amount of energy used per trip segment varied significantly (from 5 kWh to 17 kWh). This is partially explained by the conservative approach taken by the team early in the trip while still developing confidence in the vehicle and charging system (segments 1-4). Beginning with segment 5, the team began making less frequent stops as is evidenced by typical

energy usage increasing to >10 kWh per trip segment. Two exceptions to this are segments 7 and 9; on these segments, the team experienced logging errors. As a result, approximately half the data was not recorded on those segments. The final trip showed the most energy used with 17 kWh as compared to the typical 11 kWh. This was due to the team's decision to finish the last 149.7 miles in one trip segment, a much greater distance than the average segment length of 91 miles.

CONCLUSIONS

Data was collected during a cross-country trip by electric motorcycle in order to validate an energy usage model and to provide generalizations about vehicle operating parameters on such a trip. Data collected included GPS data as well as direct measurement of battery pack voltage and current. Analysis shows that the GPS-informed model predicts the measured values of energy usage to within ±5.2% on average, with precision ranging from -11.2% to 10.9%. The total energy required for the 2,366 mile trip was measured to be 270.6 kWh, or 0.114 kWh per mile. In addition, speed, power usage, and road grade data for the entire trip were summarized in histograms to show the frequency distribution of these parameters. A cursory review of the data indicates that travel speed can be characterized as 60 MPH, power draw can be characterized as 7,000W, and that road grade was in the range of ±5%. Plans for further work include dynamometer testing to improve confidence in the efficiency estimate and mining of climatological data for data related to air density, wind speed, and wind direction. Coast down tests to provide confidence in the drag coefficient value will be undertaken as the opportunity presents.

ACKNOWLEDGEMENTS

The authors thank Brian Richardson of Moto-Electra for providing access to the motorcycle during the cross country event, John Wild, Engineering lab manager at James Madison University for his help and support before and during the event, and engineering student John Edinger for his efforts preparing the auxiliary battery pack for the event. This research was supported in part by a grant from the 4-VA consortium.

REFERENCES

[1] Bae, H., Ryu, J. and Gerdes, J., 2001, "Road grade and vehicle parameter estimation for longitudinal control using GPS". Proc. of IEEE Conference on Intelligent Transportation Systems.

[2] Hart, P. M., 2010, "Estimation of Truck Drag Forces from Roll-Down Testing", International Heavy Vehicle Symposium, Melbourne, AU

[3] Hallmark, S., and Qiu, Y., 2012, "Comparison of On-Road Emissions for B-0, B-10, and B-20 in Transit Buses", Journal of the Air & Waste Management Association Vol. 62, Iss. 4.

[4] Prins, R., Hurlbrink, R., and Winslow, L., 2013, "Electric Vehicle Energy Usage Modeling and Measurement", International Journal of Modern Engineering, Vol. 13, No. 1.

[5] Gillespie, T. D., 1992, Fundamentals of Vehicle Dynamics. Society of Automotive Engineers Warrendale, PA, USA.

[6] Cossalter, V., 2006, Motorcycle Dynamics, LULU, Raleigh, NC, USA.

[7] Baddeley, G., 2001,"GPS – NMEA sentence information." http://aprs.gids.nl/gps, accessed July 7, 2013.

[8] Hi Performance Electric Vehicle Systems. 2012-2013. http://www.hpevs.com/, accessed July 26, 2013

ASME District F - Early Career Technical Conference Proceedings
ASME District F - Early Career Technical Conference, ASME District F – ECTC 2013
November 2 – 3, 2013 - Birmingham, Alabama USA

ON MAXIMIZATION OF NOISE TRANSMISSION LOSS IN MUFFLERS BY GEOMETRY MODIFICATION CONCEPT

Mostafa Ranjbar
Department of Mechanical Engineering
Eastern Mediterranean University
Gazimagusa, Turkish Republic of North Cyprus

Milad Kermani
Department of Mechanical Engineering
Eastern Mediterranean University
Gazimagusa, Turkish Republic of North Cyprus

ABSTRACT

Mufflers are designed to reflect the sound waves produced by the engine in such a way that they partially cancel themselves out. Muffler performance depends on its geometry to reduce the inlet exhaust pressure. Transmission loss (TL) is a representative factor for the measurement of the sound attenuation in mufflers. In this work, we use three-point method to calculate the TL in a specific Muffler. The areas of inlet and outlet tube will be modified to increase the TL. The relation between the geometry of the Muffler and the amount of TL in different cases will be reported.

INTRODUCTION

One of the first textbooks on the acoustics of ducts and mufflers was written by M. L. Munjal [1]. Then, several researches were done on the calculation of TL in mufflers by various methods like three-point method and four-pole method; see [2-5, 7, 10]. Wu et. al. studied muffler performance by direct mixed-body Boundary Element Method (BEM) and a three-point method for evaluating TL in packed silencers [2,4]. They also reported the BEM analysis of mufflers with an improved method for deriving the four-pole parameters [3]. Tao and Seybert reviewed the techniques for measuring muffler transmission loss [5].

Z. Cui et al. showed that the four-pole method introduces prominent parameters which are more useful, when multi silencers are connecting to each other, than the three-pole method [7].

Ranjbar et al. introduced a comparative study on methods for optimization in structural acoustics [6]. They also developed the concept of geometry optimization of mechanical structures with respect to their structural acoustic properties [8, 10].

In this paper, we perform a study on the relation of TL with the geometry of muffler. A self-written code is used to calculate the TL for various geometries of a muffler. Then the results are compared with the outputs from a code which is developed by T. Wu, i.e. MAP [10]. A simple muffler is considered for the case study. The maximum amount of TL for various types of geometries of muffler in the related frequency is calculated and reported.

PROBLEM DEFINITION

In this article, we use the three-point method to measure the muffler TL. This method considers two points on the input and one point on the output tube of a muffler. The location of these points is considered from the left edge of the inlet tube of the muffler. The impulse of the inlet tube is provided by velocity or pressure, while an anechoic termination is utilized at the outlet end [7]. Let x_1 and x_2 be the two points along the muffler center axis, respectively. Also, p_1 and p_2 are the corresponded sound pressures at those two points, which can be written:

$$p_1 = p_{ref} \cdot \frac{x}{x_1} \quad (1)$$

$$p_2 = p_{ref} \cdot \frac{x}{x_2} \quad (2)$$

p_{ref} is the reference sound pressure at a point very close to the inlet. The differences between original inlet fluid pressure and the point close to the inlet are ignored. Also, the value of x is the very close to the measuring points, and p_i is the pressure of the incoming wave:

$$p_i = \frac{1}{2i\sin[k(x_2-x_1)]}\left(p_1 e^{ikx_2} - p_2 e^{ikx_1}\right) \quad (3)$$

Also, $k = {}^{\omega}/_{c}$ denotes the wave number, c is the sound velocity, $\omega = 2\pi f$ is the pulsation frequency. Note that $\sin[k(x_2 - x_1)] \neq 0$. In this case p_i is the input pressure.

The pressure at the first and second points, i.e. p_1 and p_2, are considered in the coordinates x_1 and x_2 respectively; see figure 1. Also, the third point can be selected at any location in the outlet tube, and the pressure at that point is p_3. Then, the TL equation can be computed by:

$$TL = 20\log_{10}\left(\frac{|p_i|}{|p_3|}\right) + 10\log_{10}\left(\frac{S_i}{S_o}\right) \quad (4)$$

where S_i and S_o are the inlet and outlet tube areas. Indeed, it can be simpler rather than the above equation by considering

the diameters of areas only, unless the areas have various shapes with each together:

$$TL = 20\log_{10}\left(\frac{|p_i|}{|p_3|} \times \frac{d_i}{d_o}\right) \quad (5)$$

This state of three-point method makes the calculation of TL easy by BEM. However, the four-pole method produces the transfer matrix, which contains important parameters when the muffler has a connection to other mufflers.

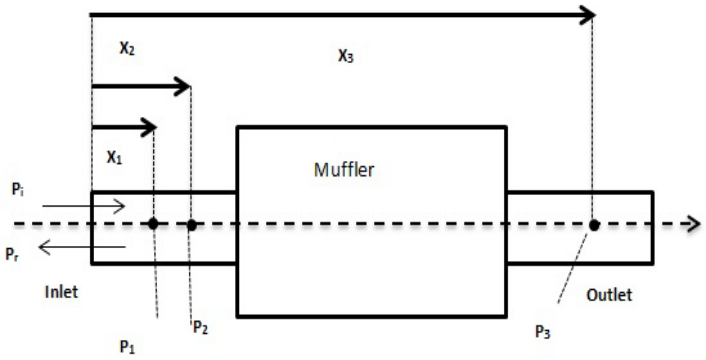

Figure 1. The three-point method

RESULTS

The initial settings for the first case study used in the self-written code are shown in table 1. The values of TL over a specific frequency range from zero to 3000 Hz are evaluated. In this case, the three-point method is used. The reference sound pressure for the fluid, i.e., air, is considered as p_{ref} = 20 μPa. The diameters of inlet and outlet tubes, i.e., d_1 and d_2, are considered as 1.375 inches. Furthermore, point 1 is 0.3 inches away from the inlet (x_1= 0.3), point 2 is 2.3 inches away from inlet (x_2= 2.3), and point 3 is 0.3 inches away from the outlet (x_3= 0.3).

Table 1. Initial settings for the first case study

P_{ref}	d_1	d_2	X_1	X_2	X_3
20 μPa	1.375 inches	1.375 inches	0.3 inches	2.3 inches	15.95 inches

The code is flexible to calculate the TL of a muffler with any arbitrary shape by using three-point method. It predicts the TL with respect to the diameters, measuring points' positions, and pressures.

In figures 2 to 7, the TL curve on the frequency range of 0 to 3000 Hz for different diameter values of inlet and outlet are shown. These results are calculated by the self-written code.

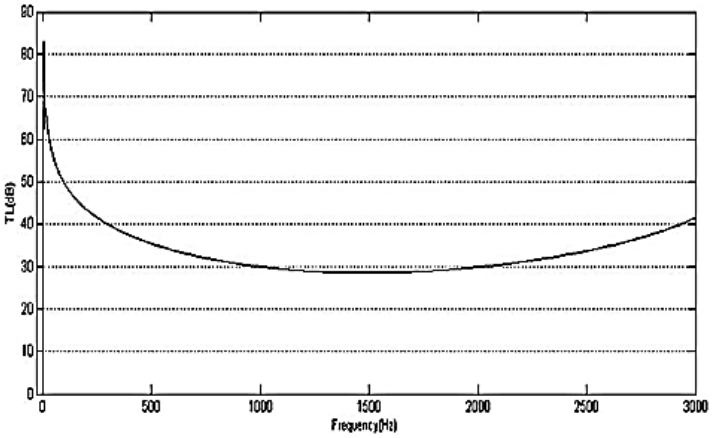

Figure 2. TL result calculated by the self-written code

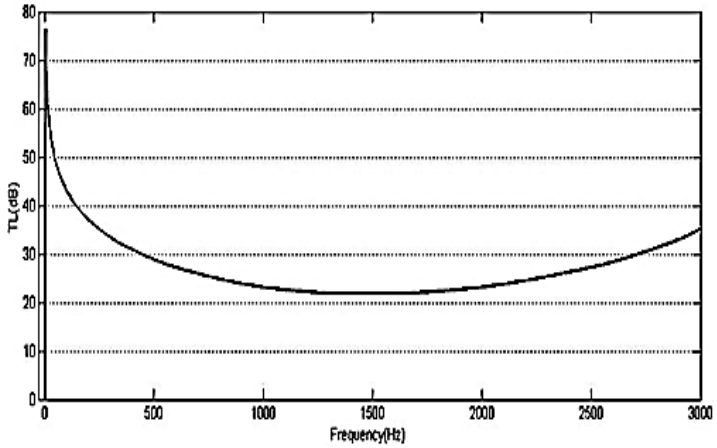

Figure 3. TL result calculated by the self-written code, Only outlet diameter is changed to 3 inches

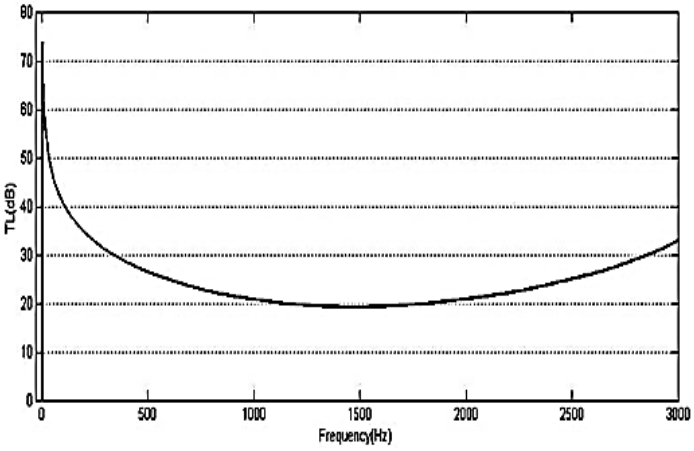

Figure 4. TL result calculated by the self-written code, Only outlet diameter is changed to 4 inches

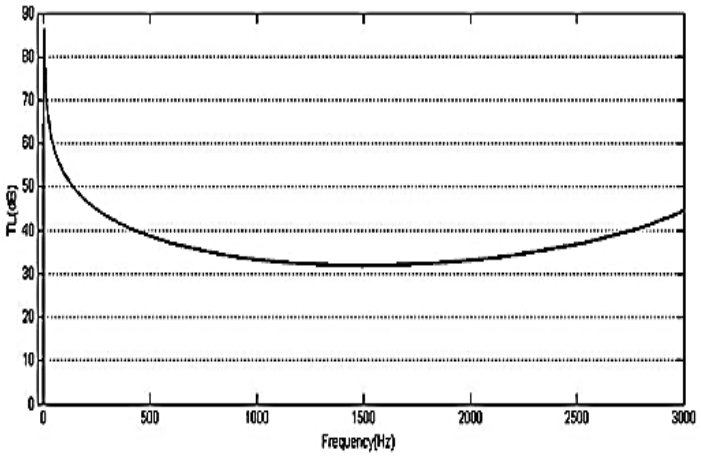

Figure 5. TL result calculated by the self-written code, Only inlet diameter is changed to 2 inches

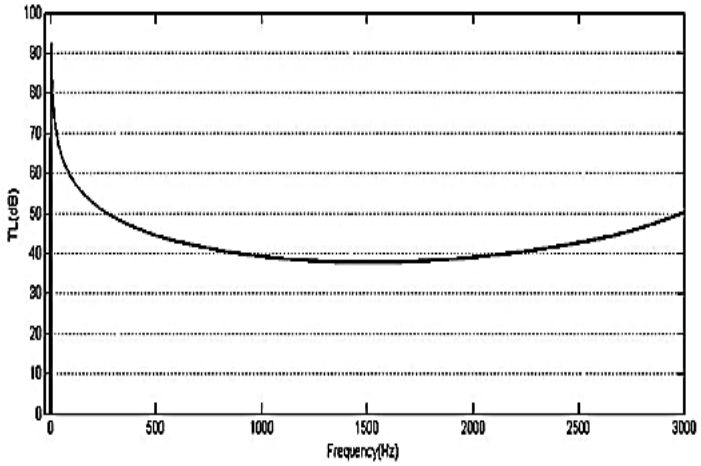

Figure 6. TL result calculated by the self-written code, Only inlet diameter is changed to 4 inches

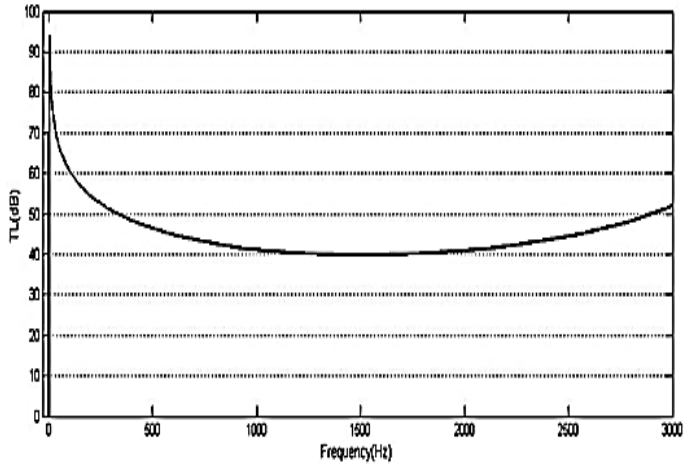

Figure 7. TL result calculated by the self-written code, Only inlet diameter is changed to 5 inches

In fig. 2, it is shown that the maximum TL is 83 dB and it occurred at the frequency of 2 Hz. It is clear that in other cases, which are shown in figures 2 to 7, the frequency of maximum TL is similar. Just the values of maximum TL are changed to 76.3 dB, 73.8 dB, 86.2 dB, 92.1 dB and 94.08 dB in the figures 3 to 7, respectively. Furthermore, the highest averaged value of TL over the whole frequency range is 44.75, and it occurs in figure 7 for the case when the inlet diameter is changed to 5 inches. Also, the lowest averaged TL value is for the case in which the outlet diameter is changed to 4 inches. In fact, increasing the value of the inlet diameter will result in an increase to the value of TL. But, with increasing the outlet diameter, the maximum and averaged TL will decrease.

As the second example, a comparative study is done in between the result from the self-written code and the results from the MAP [9] software. MAP is written by T. Wu at the University of Kentucky to calculate the TL for various muffler shapes using BEM.

In figures 8 and 9, the TL calculated by the MAP and our self-written code are presented. Here, a bulk is considered and the pressures were chosen arbitrarily. The inlet and outlet radiuses are 6 inches, i.e. $R1 = R2$, and the coordinate of point 1 is selected as zero (X_1=0). Furthermore, point 2 has X_2=3 inches, and point 3 is 29.99 inches from inlet area (X_3= 29.99). In figure 8, the logarithmic measure of TL calculated by MAP is shown. Also, the similar result from the self-written code is shown in figure 9. It is shown in figure 8 that the maximum TL is about 48 dB in the frequency of 2000 HZ. However, in figure 9 it is shown that the maximum TL, i.e. 48 dB, is at the frequency of 2100 Hz.

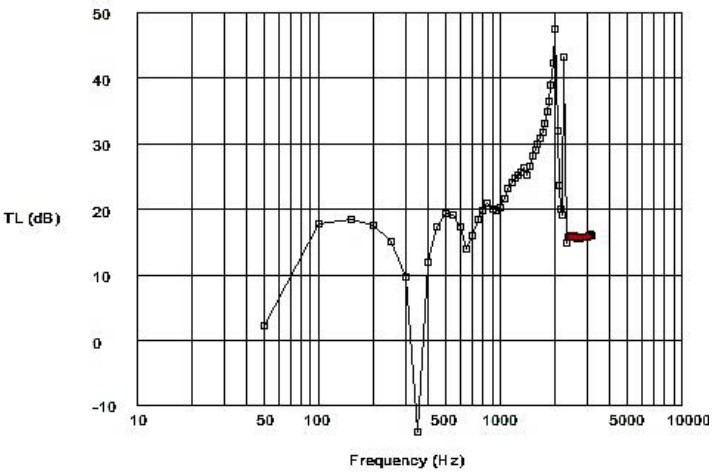

Figure 8. TL result from MAP software

There are some differences between the results calculated by our self-written code and the MAP software; see figures 8 and 9. In the following, some clarifications in this context are presented.

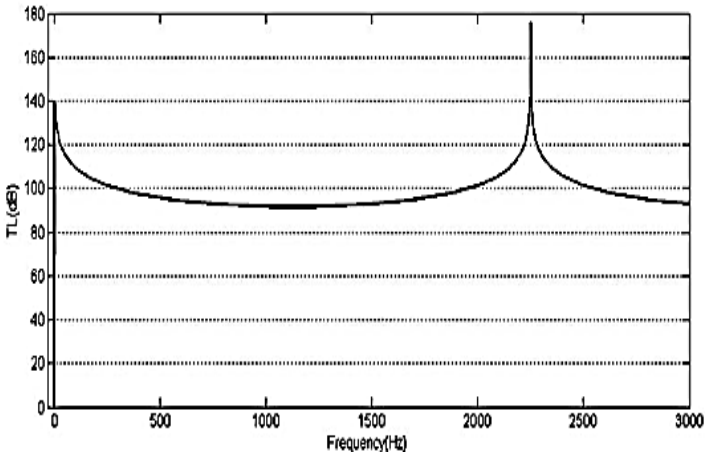

Figure 9. TL result calculated by the self-written code with the same initial setting as MAP software

The three-point method is based on considering the position of three points. MAP has two options as settings for considering the three points' positions. In fact, differences will appear in auto adjustment, which impact the decision whether to consider two points, while one of them is zero completely, or whether the system should evaluate the points according to other types of equations. Consequently, thinking over the zero amounts, shows us that the positions of the points are not important enough for calculation of TL by MAP. Although in Manual setting, it would be possible for the user to change the positions of points, the desired result is not shown. However, in our self-developed code, the user will have the chance to give the desired distances and see the impacts of them on TL values. In MAP, when the considered fluid is Air, it ignores the sound velocity, while if it is utilized Refrigerant, the sound velocity will be scored. The speed of sound has significant influence on increasing the amount of TL in some parts.

SUMMARY AND CONCLUSION

In this paper, our aim was to modify the shape of the inlet and outlet of a muffler. In this regard, we developed a self-written software to calculate the value of TL for different shapes of mufflers. Here, we follow the traditional three-point measurement of a TL without silencer by computing the sound pressure level. The lengths of the tubes, the measuring points' position, and the diameter of inlet and outlet areas, are the most important parameters in this case. If the lengths of the tubes increase and the positions of the three points come closer to the entrances of the inlet tube and outlet of the silencer respectively, then the TL starts to increase in most parts of the frequency ranges.

Consider that if the diameters of the inlet and outlet areas are the same or equal, they will have no effect to change the amount of TL. If the inlet area increases and the outlet area is fixed, then the total amount of TL will increase. Furthermore, if the inlet is fixed and the outlet area is increased, then the total amount of TL is decreased. By perusing among the results, it is specified that increasing inlet diameter has the most significant influence on maximization of TL and it can be a spotlight for designing the shape of mufflers. For practical applications, it is better to modify the geometry of muffler when a narrow-band frequency, e.g., 200 Hz 1/3 octave band, for the maximization of TL is considered. In fact, the maximization of TL over a wide frequency range is not useful for the real applications. This issue should be investigated in future works. Then, more efforts should be put on the shape modification of the muffler by various optimization strategies

ACKNOWLEDGMENTS

The evaluation version of MAP software is used in this study. MAP is developed by T. W. Wu from the University of Kentucky, USA.

REFERENCES

[1] Munjal, M. L., 1987, Acoustics of Ducts and Mufflers, New York: Wiley-Interscience.

[2] Wu, T. W., and Wan, G. C., 1996, "Muffler Performance Studies Using a Direct Mixed-Body Boundary Element Method and a Three-Point Method for Evaluating Transmission Loss," ASME Transactions, J. Vib. And Acoust., 118, pp. 479-484.

[3] Wu, T. W., Zhang, P., and Cheng, C. Y. R., 1998, "Boundary Element Analysis of Mufflers With An Improved Method For Deriving The Four-Pole Parameters," Journal of Sound and Vibration, 217 (4), pp. 767-779.

[4] Wu, T. W., Cheng, C. Y. R., and Zhang, P., 2002, "A Direct Mixed-Body Boundary Element Method for Packed Silencers," J. Acoust. Soc. Am., 111, pp. 2566-2572.

[5] Tao, Z., and Seybert, A. F., 2003, "A Review of Current Techniques for Measuring Muffler Transmission Loss," SAE International.

[6] Ranjbar, M., Hardtke, H.-J., Fritze, D., and Marburg, St., 2010, "Finding the Best Design within Limited Time: A Comparative Case Study on Methods for Optimization in Structural Acoustics," Journal of Computational Acoustics, 18(2), pp. 149-164.

[7] Cui, Z., and Huang, Y., 2012, "Boundary Element Analysis of Muffler Transmission Loss with LS-DYNA," 12th International LS-DYNA® Users Conference.

[8] Ranjbar, M., Marburg. St., Hardtke, H.-J., 2012, "Structural-Acoustic Optimization of a Rectangular Plate: A Tabu Search Approach", Journal of Finite Elements in Analysis and Design, 50, pp. 142-146.

[9] Wu, T. W., 2012, "MAP V0.90 User's Guide," University of Kentucky, USA.

[10] Ranjbar, M., Marburg. St., Hardtke, H.-J., 2013, "Vibroacoustic Optimization of Mechanical Structures: A Controlled Random Search Approach," Advanced Material Research, 622-623, pp. 158-161.

COOLING CHANNEL ANALYSIS TO ENHANCE THE EFFICIENCY OF FUEL CELLS AND PHOTOVOLTAIC PANELS

Ernandes Jose Goncalves do Nascimento
Department of Mechanical Engineering and
Center of Advanced Power Systems
Florida State University
Tallahassee, FL, USA

Obiechina Iruka Abakporo
Department of Mechanical Engineering and
Center of Advanced Power Systems
Florida A&M University
Tallahassee, FL, USA

Alejandro Rivera
Department of Mechanical Engineering and
Center of Advanced Power Systems
Florida State University
Tallahassee, FL, USA

Juan Ordonez
Department of Mechanical Engineering and
Center of Advanced Power Systems
Florida State University
Tallahassee, FL, USA

ABSTRACT

The overheating of cells in alternative energy technologies significantly decreases the efficiency and lifespan of the device. This project is aimed at developing improvements to current fuel cell and solar panel prototypes currently being used. As a starting point, cooling channels and heat sinks for photovoltaic (PV) panels were simulated under various circumstances using COMSOL Multiphysics and Matlab software to thoroughly analyze the methods that will maintain and/or achieve the optimum power output. The emphasis of this project is the heat transfer analysis of the cooling methods that is examined through simulation. The focus is placed on forced convection cooling here, but natural convection will also be considered and accounted for in the future. Optimized power production by the PV is calculated as a function of the number of fins (N), fin spacing (a), and air flow velocity (v). Air is the primary fluid used for cooling due to both natural availability and abundance. Heat transfer analysis is essential to the development and implementation of alternative technologies on a global scale. The results obtained from this project show that photovoltaic panels, fuel cells, and potentially other alternative energy technologies can in principle, be effectively cooled quite easily, reinforcing the versatility, longevity, and dependability of these applications.

INTRODUCTION

Since being introduced as a means of harnessing energy photovoltaic modules (solar panels or photovoltaic panels) have been subjected to the discussion of relatively low efficiency (highest PV panel efficiencies currently available on the market are below 23% of energy conversion) and how possible improvements can turn solar cells into a more viable system for electricity production. It is well known that the efficiency of photovoltaic solar cells increases with a decrease in the operating temperature because higher resistance introduces a new concept called PV Thermal (PV/T), which seems to be spreading fast on the market. The PV/T system is a solar hybrid solar collector that is capable of simultaneously producing two types of energy largely used by consumers: electricity and low temperature heat. This task can be achieved by circulating a colder fluid (water or air) inside or outside of a PV Panel; this can be accomplished by either forced or natural convection [7]. Part of the solar radiation is absorbed by the photovoltaic cells and is converted into electricity, while part of the heat excess is dissipated to the circulating fluid, causing the operating temperature to decrease. A less sophisticated system can be built using the same PV/T idea with the difference that the energy acquired by the fluid is wasted to the environment. Instead of using a complex and expensive solar collector, only a simple heat sink is needed for improved heat transfer.

The focus of this project is to model and simulate a simple-to-build system for heat extraction in a SOLARA-SM200S photovoltaic panel using an aluminum heat sink with rectangular fins. The PV Panel that is utilized during the study is shown in Figure 1.

Modeling and optimizing a heat sink capable of transferring heat from a solid to a fluid with relatively good efficiency requires knowledge in the physical equations related to the analysis of heat transfer and fluid mechanics. For the cases stated in this study, heat transfer equations for solids and

Figure 1: Photovoltaic Panel used in the project.

fluids are used. These simulations and calculations will be executed using COMSOL, while Matlab and Excel will be used to produce the graphs.

MATHEMATICAL ANALYSIS

The first law of thermodynamics (commonly referred to as the principle of conservation of energy) is the fundamental law responsible for all heat transfer [1]. However, internal energy, U, is a rather inconvenient quantity to measure and use in simulations and for that reason the equation is usually rewritten in terms of temperature, T. The resulting heat equation for a fluid is given as:

$$\rho C_p \left(\frac{\partial T}{\partial t} + (u \cdot \nabla)T\right) = -(\nabla \cdot q) + \tau : S - \frac{T}{\rho}\frac{\partial p}{\partial T}|_p \left(\frac{\partial p}{\partial T} + (u \cdot \nabla)p\right) + Q \quad (1)$$

where (including the SI units):

- ρ is the density (kg/m^3);
- C_p is the specific heat capacity at constant pressure (J/(kg*K));
- T is absolute temperature (K);
- **u** is the velocity vector (m/s);
- **q** is the heat flux by conduction (W/m^2);
- p is pressure (Pa);
- τ is the viscous stress tensor (Pa);
- **S** is the strain-rate tensor (1/s):

$$S = \frac{1}{2}(\nabla \mathbf{u} + (\nabla \mathbf{u})^T) \quad (2)$$

- **Q** contains heat sources other than viscous heating (W/m^3).

A number of thermodynamic relations were used for deriving equation (1). It was also assumed that mass is a constant, which means that density and velocity are governed by the relation:

$$\frac{\partial p}{\partial t} + \nabla \cdot (\rho v) = 0 \quad (3)$$

Viscous heating of a fluid is represented by the second term on the right of equation (1). An equivalent equation arises from the internal viscous damping of a solid. The operation ":" is a contraction and is expressed as:

$$\boldsymbol{a} : \boldsymbol{b} = \sum_n \sum_m a_{nm} b_{nm}$$

Fourier's law of heat conduction was used by the heat transfer interfaces on COMSOL, stating that the time rate of heat transfer through a material is proportional to the negative gradient in the temperature and to the area, at right angles to that gradient, through which the heat is flowing. The law can be stated in two equivalent forms: the integral form (the amount of energy flowing into or out of a body is analyzed as a whole) and the differential form (flow rates or fluxes of energy are analyzed locally). The differential form is mathematically expressed as the equation below.

$$\vec{q} = -k\nabla T \quad (4)$$

where (including the SI units):

$\vec{q}$ is local heat flux vector, (W/m^2);
k is material thermal conductivity, (W/m*K);
∇T is the temperature gradient, (K/m).

In a solid, the thermal conductivity (k) can be anisotropic (the material has different thermal conductivity properties for different directions). Then k becomes a tensor matrix:

$$k = \begin{bmatrix} k_{xx} & k_{xy} & k_{xz} \\ k_{yx} & k_{yy} & k_{yz} \\ k_{zx} & k_{zy} & k_{zz} \end{bmatrix} \quad (5)$$

And in this case, the conductive heat flux is given by the following equation:

$$q_i = -\sum_j k_{ij} \frac{\partial T}{\partial x_j} \quad (6)$$

Pressure work is represented by the third term of equation (1). This quantity is also responsible for the heating of a fluid under adiabatic compression and some thermoacoustic effects.

It is usually small for low Mach number flows and a similar term can be included to take into consideration thermoelastic effects in solids.

Equation (6) can be replaced into equation (1) and after reordering the terms and ignoring viscous heating and pressure work, the heat equation becomes:

$$\rho C_p \frac{\partial T}{\partial t} + \rho C_p \boldsymbol{u} \cdot \nabla T = \nabla \cdot (k \nabla T) + Q \qquad (7)$$

Equation (7) is solved for the temperature, ***T***, in the Heat Transfer in Fluids feature on COMSOL [2]. Then, the equation governing pure heat transfer (8) can be obtained by just setting velocity to zero.

$$\rho C_p \frac{\partial T}{\partial t} + \nabla \cdot (-k \nabla T) = Q \qquad (8)$$

The heat flux (thermal flux) is the rate of heat energy transfer through a unit of area in a given surface. In this project a constant general inward heat flux value was set for all simulations to represent the amount of solar radiation developed into heat. The following equation was used in the heat flux interface in COMSOL:

$$-\boldsymbol{n} \cdot (-k \nabla T) = q_0 \qquad (9)$$

The solar radiation during the afternoon on the Equator's line (zero degrees latitude) is about 1000 W/m^2 [4]. As Tallahassee is somewhere close to 30° latitude north of the Equator's line it has a lower index of solar radiation reception and a larger variation in a year due seasonal effects. As there is no exact value for the solar radiation level, a reasonable and fixed value of 870 W/m^2 [4] was used for calculating the radiation flux that is developed into heat flux in the PV Panel.

Calculating the radiation flux that is developed into heat flux by the PV Panel

$$\dot{Q}_{Heat} = I_{Tallahassee} - \dot{Q}_{Reflected} - \frac{\dot{W}_{PV}}{A_{PV}} \qquad (10)$$

$$\dot{Q}_{Heat} = I_{Tallahassee} - a * I_{Tallahassee} - \frac{\dot{W}_{PV}}{A_{PV}}$$

$$\dot{Q}_{Heat} = 870.0 \frac{W}{m^2} - 0.30 * 870.0 \frac{W}{m^2} - \frac{50\ W}{0.44 * 1.02\ m^2}$$

$$\dot{Q}_{Heat} = 497.592 \frac{W}{m^2}$$

Due to the value above being an approximation to the real radiation rate developed into heat, the value used as one of the parameters for the simulation in COMSOL will be rounded to 500.0 W/m^2.

When modeling heat transfer problems, it is common to have boundary conditions for a fluid cooling a surface by natural or forced convection. It is possible to model this process on COMSOL in two ways:

1) Use a heat transfer coefficient on the convection-cooled surfaces;
2) Extend the model to describe the flow and heat transfer in the cooling fluid.

In the scenario of a complex geometry or external flow, the second approach is the correct one. The "Conjugate Heat Transfer" interface on COMSOL exists for this purpose and it was used in all simulations performed in this project. The geometry studied started to get complicated after reaching a certain number of fins, therefore exercising the first option would not be recommended. Also, it would require experimental work for determining the correct value for the heat transfer coefficient, which can be difficult. That coefficient depends on the cooling fluid, the fluid's material properties, and the surface temperature—and, for forced-convection cooling, also on the fluid's flow rate. In addition, the geometrical configuration affects the coefficient. Although extending the model to describe the flow and heat transfer in the cooling fluid is the appropriate approach, it does have some negative points such as increasing the costs of simulations due to the high computational performance and amount of memory required to compute.

Heat transfer between a fluid and a solid surface at different temperatures (convective heat transfer) is classified according to the nature of the fluid's flow. The following equation governs all of the external convection:

$$-\boldsymbol{n} \cdot (-k \nabla T) = h \cdot (T_{ext} - T) \qquad (11)$$

Where (including the SI units):

$\boldsymbol{n}$ is the orientation vector;
∇T is the temperature gradient, (K);
k is material thermal conductivity, (W/m*K);
h is convective heat transfer coefficient, (W/m^2*K);
T_{ext} is external temperature, (K);
T is surface temperature, (K).

The convective heat transfer coefficient is calculated by COMSOL as a function of the plate diameter (area/perimeter), external fluid's properties, absolute pressure and external temperature.

For the purpose of this project it is possible to infer that the theoretical heat sink assembled to the PV Panel experiences both conductive and forced convective heat transfer. When the solar radiation hits the PV Panel, part of it is reflected into the atmosphere, another part is absorbed, and the remaining part is converted by the photovoltaic cells into electricity. The absorbed solar radiation produces large amounts of heat that can be translated as a solar heat transfer flux (W/m^2) in the top side of the PV Panel. This value can be estimated using the albedo factor (also known as radiation reflection coefficient) for solar photovoltaic cells. In this case, the albedo coefficient depends on the color of the panel (usually black or blue). Most PV Panels have an albedo around 0.3 or 30% of radiation reflection (it increases if it is blue, and decreases if it is black). Table 1 below contains important information about the PV Panel used in this study.

Table 1: Solar Panel Technical Specifications.

Brand	SOLARA
Model	SM 200 S
Origin	Germany
Performance	200 Wh/d
Power (P_{mpp})	50 Wp +/- 10%
System Voltage	12 V
Voltage (V_{mpp})	17,8 V
Open circuit voltage (U_{OC})	21,7 V
Current (I_{mpp})	2,8 A
Short circuit current (I_{OC})	2,98 A
Estimated Albedo Factor (a)	0.30
Area	0.449 m^2

The Finite Element Method is the numerical technique applied by COMSOL for finding approximate solutions to boundary value problems. By using variation methods (calculus of variations) the software is capable of minimizing an error function and produces a stable solution. The main idea of FEM is analogous to the idea of approximating a larger circle by connecting many tiny straight lines. The application of the FEM most commonly consists in filling with triangles the surfaces of a two or three dimensional geometry eventually creating a mesh. In addition, FEM connects many simple element equations over many small subdomains, named finite elements, to approximate a more complex equation over a larger domain. The number of finite elements used for filling a domain is commonly referred to as the refining of the mesh. A higher number of finite elements will result in more accurate calculations on the refined region; however a higher CPU effort will be required.

The three dimensional geometry (shown in Fig. 2) developed in COMSOL was used for all of the PV simulations.

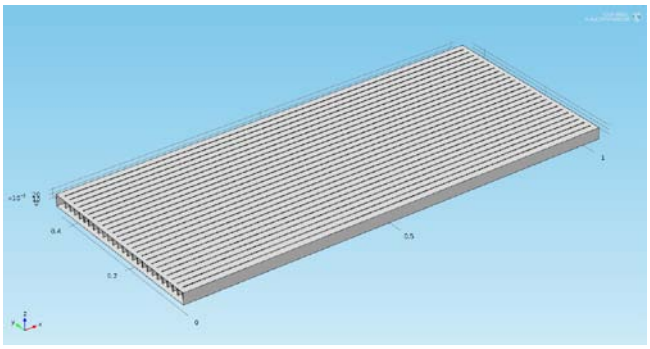

Figure 2: Three dimensional view of the geometry used in COMSOL.

The dimensions for the frame were acquired in the laboratory by taking experimental measurements by metric tape. The dimensions of the fins were based on the PV Panel's structure values. All values obtained are shown in Table 2.

Table 2: Dimensions of the Geometry.

Geometry	Width (m)	Height (m)	Extrusion Distance (m)
Fins	0.002	0.027	1.000
PV Panel's Frame	0.440	0.027	1.020

CONDITIONS ADOPTED IN SIMULATIONS

The simulations performed had several conditions adopted for simplifying the optimization problem and reducing the average simulation time. The assumptions made on the simulations presented on this project were considered as follows:

- Radiation heat transfer between the geometry and its own surfaces was neglected;
- Constant thermal conductivity was adopted for aluminum;
- Uniform heating by the solar heat flux;
- Steady state;
- Constant ambient temperature of 298.15 K;
- Constant ambient pressure of 1 atm ($1.0133x10^5$ Pa);
- PV Panel (photovoltaic cells, frame and the heat sink) was considered to be 100% aluminum.

MODELING AND SIMULATION

Both convection cases can be built using a very simple heat sink that mainly consists of thin rectangular fins made out of aluminum.

Parameters

A list containing all of the important values (dimensions, constants, fins coordinates, expression and number of fins) for the parameters was created in Excel and imported into COMSOL (shown in Table 3).

Table 3: List of parameters used in the simulations.

Parameters

Name	Expression	Value	Description
PV_Width	0.44[m]	0.44000 m	PV Panel Width
PV_Height	0.027[m]	0.027000 m	PV Panel Height
F_Width	0.002[m]	0.0020000 m	Fin Width
F_Height	0.027[m]	0.027000 m	Fin Height
T0	298.15[K]	298.15 K	External Air Temperature
patm	1[atm]	1.0133E5 Pa	Air Pressure
ext1	1.0[m]	1.0000 m	First Extrusion
ext2	1.02[m]	1.0200 m	Second Extrusion
theta	30	30.000	Tilt angle
Num_Fins	70	70.000	Number of Fins
Spa_Fins	(PV_Width)/(Num_Fins+1)	0.0061972 m	Spacement of the Fins
r1	1	1.0000	Coordinate of the Fin
r2	2	2.0000	Coordinate of the Fin
r3	3	3.0000	Coordinate of the Fin
r4	4	4.0000	Coordinate of the Fin
r5	5	5.0000	Coordinate of the Fin

Materials

The material used to build the whole PV Panel structure and fins is the Aluminum 3003 – H18 alloy and Air was used as a fluid. Both materials have all its constants and properties already defined in COMSOL.

Forced Convection Boundary Conditions

Conjugate Heat Transfer Physics was used in the Forced Convection problem and several boundary conditions were assumed. A list containing all condition and setting values is below:

- Heat Transfer in Solids;
- Thermal Insulation;
- Wall;
- Initial Values (Temperature set to T0 = 298.15 K);

All the conditions above are added by default in the Conjugate Heat Transfer Module. The following conditions were manually added to the model:

- Fluid;
- Inlet (Air flow entrance, set to laminar inflow, entered average velocity according to simulation and entrance length = 0.44m);
- Outlet (Air flow exit, set to pressure, no viscous stress and pressure = 0 Pa);
- Outflow;
- Heat Flux (Solar radiation developed into heat, set to general inward heat flux, q = 500.0 W/m^2);
- Temperature (Air entrance temperature, set to T0 = 298.15 K);
- Convective Cooling 1 (Heat transfer coefficient set to External natural convection - Horizontal plate upside, External temperature = 298.15 K);
- Convective Cooling 2 (Heat transfer coefficient set to External natural convection – Vertical wall, External temperature = 298.15 K);
- Convective Cooling 3 (Heat transfer coefficient set to External natural convection - Horizontal plate downside, External temperature = 298.15 K).

Mesh

The simulations required good refinement of the finite elements in the mesh to acquire acceptable results. Physics controlled mesh and the *"coarser"* setting was used due to the computer limitations. Some of the more important parameters to obtain from the mesh compilation are number of elements, minimum element quality, and average element quality. These values are displayed below in Table 4 and the geometry viewed in Fig 4.

Table 4: Important Mesh Statistics.

Parameters:	50 Fins:	70 Fins:
# of Elements	413,082	912,888
Avg. Element Quality	0.2686	0.2496
Minimum Element Quality	0.003239	7.691E-4

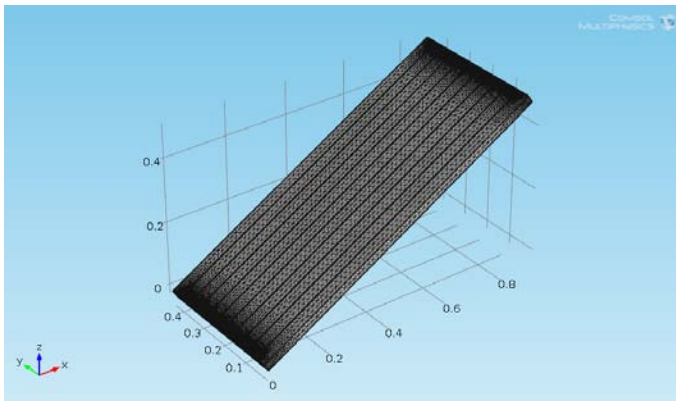

Figure 3: Three dimensional view of the mesh used.

RESULTS

The results obtained in the simulations performed in COMSOL were used for calculating several variables. Below are the equations and summary how the calculations were performed.

- Calculating the PV Panel Efficiency as a function of the Temperature, $\boldsymbol{\eta_{pv}}$ [7]

$$\eta_{pv} = f(T_{pv})$$
$$\eta_{pv} = 0.147 - 0.0008T_{pv} \quad (12)$$

- Calculating the PV Panel Power, $\boldsymbol{\dot{W}_{pv}}$ (W)

$$\eta_{pv} = \frac{\dot{W}_{pv}}{I_{Solar}A}$$
$$\dot{W}_{pv} = \eta_{pv} I_{Solar} A \quad (13)$$

- Calculating the Pipe Pressure Drop, Pp (Pa)

A pipe pressure drop was added to the calculations in order to give more realism to the project. A reasonable value of 20 Pa was considered when calculating the power required by the fan for all Forced Convection cases.

- Calculating the Fan Power, $\boldsymbol{\dot{W}_{fan}}$ (W)

Most fans have a rate of energy conversion around 60% of efficiency. A fan efficiency (η_{fan}) of 40% of energy conversion was assumed to calculate fan power.

$$\dot{W}_{fan}\eta_{fan} = \frac{\Delta P}{\rho_{air}}\dot{m} \quad (*1) \quad (14)$$

where:

$$\dot{m} = Av\rho_{air} \quad (*2)$$

Replacing equation (*2) into equation (*1):

$$\dot{W}_{fan}\eta_{fan} = \frac{\Delta P}{\rho_{air}} Av\rho_{air}$$

$$\dot{W}_{fan} = \frac{|\Delta P| Av}{\eta_{fan}}$$

- Calculating the Total Power Produced, $\boldsymbol{\dot{W}_{total}}$ (W)

The Total Power produced is the amount of energy per second produced by the system considering the most representative theoretical loss (the power used by the fan).

$$\dot{W}_{total} = \dot{W}_{pv} - \dot{W}_{fan} \quad (15)$$

The forced convection simulations resulted in several charts with a total of eighty data points. Using the acquired results the following graphs were plotted on Excel and Matlab:

- Average Temperature versus Number of Fins (Fig 4);
- Efficiency versus Number of Fins (Fig 5);
- 3D - Total Power versus Number of Fins versus Air Flow Velocity (Fig 6).

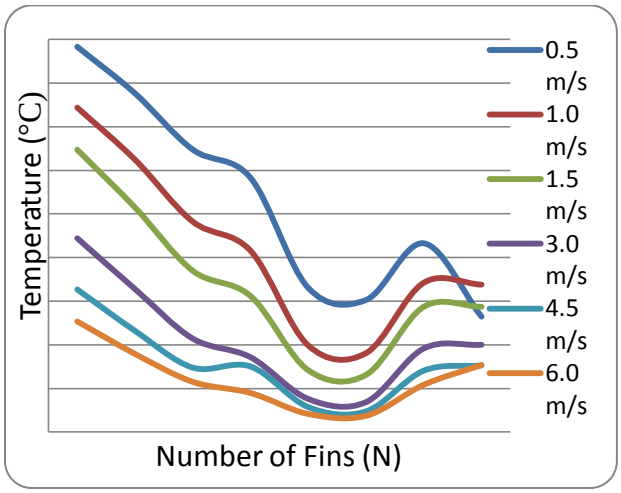

Figure 4: Average Temperature versus Number of Fins.

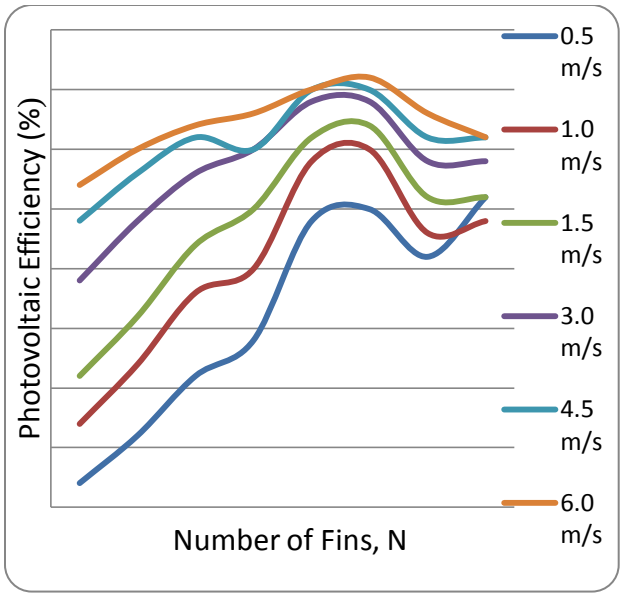

Figure 5: Photovoltaic Efficiency versus Number of Fins.

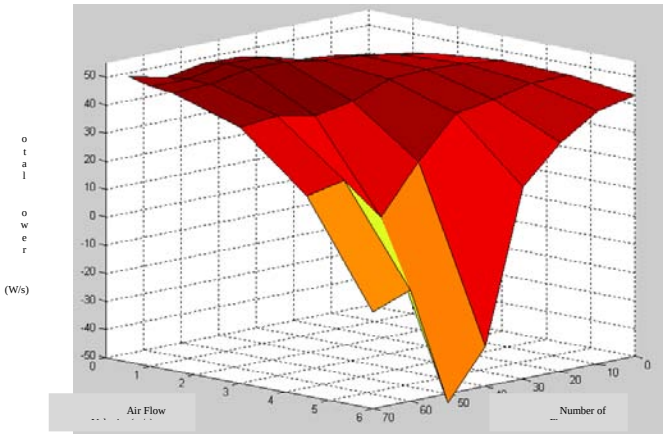

Figure 6: Total Power versus Air Flow Velocity versus Number of Fins.

The negative values of the total power (shown in Fig 6) simply indicate that there are an insufficient number of fins and/or low air flow velocity. Essentially meaning that the fan power generated exceeds the power produced by the PV panel (see Equation 15).

CONCLUSION AND FUTURE WORK

The charts developed from the PV panel-fin integrated system simulations demonstrate that greater efficiencies can be achieved via methods of forced convective cooling. The most productive systems are those of the 1.0 m/s flow velocity and 50 fin variety. Although the results obtained are even more satisfactory than previously expected, the theoretical work presented in this project should be validated experimentally just to approve/disapprove the assumptions/approximations made. Lastly, this heat transfer analysis will be applied to PEM fuel cell and other alternative energy applications.

ACKNOWLEDGMENTS

This work was supported in part by the Multi-physics of Active Systems and Structures (MASS) NSF REU Summer Program, the Office of Naval Research (ONR), and FAMU's Title III Minority Graduate Engineering Program.

REFERENCES

[1] F. Incropera, D. Dewittk, "Fundamentos de Transferencia de Calor," Quarta Edicao.
[2] "Heat Transfer Module User's Guide," COMSOL AB, 2010.
[3] J. Fontenault- Bradely, Ernesto Gutierrez- Miravete, "Modeling a Combined Photovoltaic-Thermal Solar Panel," Hartford.
[4] MacKay, David JC. "Ch 6." *Sustainable Energy- Without The Hot Air*. 3.5.2 ed. England: UIT Cambridge, 2009. 38-41. Print.
[5] Myers Et Al. "Solar Spectral Irradiance: Air Mass 1.5." *Solar Spectral Irradiance: Air Mass 1.5*. NREL, n.d. Web. 5 Aug. 2013.
[6] Woodbank Communications. "Battery and Energy Technologies." *Electricity Generation from Solar Energy, Technology and Economics*. Electropaedia, n.d. Web. 12 Sept. 2013.
[7] Tonui, J.K. *Improved PV/T Solar Collectors with Heat Extraction by Forced or Natural Air Circulation*. Tech. N.p.: Elsevier, 2006. *Improved PV/T Solar Collectors with Heat Extraction by Forced or Natural Air Circulation*. Science Direct, 4 May 2006. Web. July-Aug. 2013